High-Resolution Ultrasound and Speckle Tracking: a non-invasive approach to assess *in vivo* gastrointestinal motility during development

Pierre Sicard[1,2], Amandine Falco[1], Sandrine Faure[1], Jérome Thireau[1], Stéphanie E. Lindsey[1,3], Norbert Chauvet[1], and Pascal de Santa Barbara[1,*]

[1]PhyMedExp, University of Montpellier, INSERM, CNRS, Montpellier, France

[2]IPAM, Biocampus Montpellier, CNRS, INSERM, University of Montpellier, Montpellier, France.

[3]Department of Mechanical and Aerospace Engineering, University of California San Diego (UCSD), La Jolla, CA, USA

[*]Correspondence:

Pascal de Santa Barbara, PhyMedExp, 371 avenue Doyen Giraud, 34295 Montpellier, Cedex 5, France, Pascal.de-santa-barbara@inserm.fr, +33 (0)4 67 41 52 34

Abbreviations used in this paper

AP, anterior–posterior; bpm, beats per minute; CIPO, chronic intestinal pseudo-obstruction; $CoCl_2$, cobalt chloride; E, embryonic day; ENS, enteric nervous system; γSMA, gamma smooth muscle actin; GI, gastrointestinal; ICC, interstitial cell of Cajal; RCAS, replication-competent retroviruses; TTX, tetrodotoxin; vENCDC, vagal enteric neural crest-derived cell.

Keywords: Chick model; Gastrointestinal; smooth muscle; enteric nervous system; ultrasound echography.

ABSTRACT

Gastrointestinal motor activity has been extensively studied in adults, conversely only few studies have investigated fetal motor skills. When the gastrointestinal tract starts to contract during the embryonic period and how this function evolves during development are not known. Here, we adapted a non-invasive high-resolution echography technique combined with speckle tracking analysis to examine the gastrointestinal tract motor activity dynamics during chick embryo development. We provided the first recordings of fetal gastrointestinal motility in living embryos without anesthesia. We found that although gastrointestinal contractions appear very early during development, they become synchronized only at the end of the fetal period. To validate this approach, we used various pharmacological inhibitors and *BAPX1* gene overexpression *in vivo*. We found that the enteric nervous system determines the onset of the synchronized contractions in the stomach. Moreover, alteration of smooth muscle fiber organization led to an impairment of this functional activity. Altogether, our findings show that non-invasive high-resolution echography and speckle tracking analysis allow visualizing and quantifying gastrointestinal motility during development and highlight the progressive acquisition of functional and coordinated gastrointestinal motility before birth.

INTRODUCTION

In vertebrates, the gastrointestinal (GI) tract is essential for the absorption of water and nutrients. Early during embryo development, the GI tract is formed as a closed primitive and uniform tube, composed of endoderm and mesenchyme, that becomes regionalized along the anterior–posterior (AP) axis into various organs (esophagus, stomach, duodenum, and intestines) (de Santa Barbara et al., 2002; de Santa Barbara et al., 2003). The mesenchyme gives rise (from the outer to the inner part of the gut wall) to the longitudinal and circular smooth muscle layers, the submucosa, and the muscularis mucosae, close to the epithelial lining (Le Guen et al., 2015). The circular and longitudinal smooth muscle layers align in orthogonal orientations to ensure the gut coordinated contraction and relaxation (Huycke et al., 2019; Roberts, 2000). Concomitantly with these morphological events, the GI mesenchyme is colonized by neural crest-derived cells, a cell population that gives rise to the enteric nervous system (ENS), the intrinsic innervation of the GI tract (Burns et al., 2009). The ENS originates predominantly from vagal enteric neural crest-derived cells (vENCDCs) that delaminate from the neural tube, enter the esophageal mesenchyme, and populate the entire GI tract, from the esophagus to the terminal colon, through an AP migration wave (Burns and Douarin, 1998; Burns et al., 2000; Fairman et al., 1995; Faure et al., 2015; Le Douarin and Teillet, 1973; Yntema and Hammond, 1954). During their migration, vENCDCs proliferate and differentiate into ENS neurons and glial cells. They form two concentric plexuses of ganglion cells: the myenteric plexuses are localized in the GI wall muscle layers and control smooth muscle contraction and relaxation (Bourret et al., 2017; Chevalier, 2018; Heanue et al., 2016), whereas the submucosal plexuses lies in the submucosa and innervates epithelial cells and muscularis mucosae (Uesaka et al., 2016).

Vertebrate GI motor activity has been extensively studied in adults, but rarely during embryo development. During the prenatal period, the human GI tract digests and absorbs nutrients from the amniotic fluid and propels the meconium (Mclain, 1963). There are good clinical evidences that in late gestation, fetal growth requires an intact and functional GI tract for swallowing the amniotic fluid and for the enteral uptake of nutrients (Koppen et al., 2017; Singendonk et al., 2014). Although fetal gastric peristalsis has been observed using ultrasound imaging in humans (Sase et al., 1999), little is known about when and how digestive motor skills appear and develop during development, mainly due to the limitations of *in vivo* embryo assessment. Until now, embryonic gut motility has been studied only in organ culture systems. However, depending on the GI segment and preparation method (open, tubular, muscle strips), the motility patterns and contractile behavior can be biased by the apparatus used to measure smooth muscle contractility (Barnes et al., 2014). Various invasive approaches using different dissected GI segments for organ culture showed that embryonic GI segments can contract autonomously or upon stimulation (Roberts et al., 2010). These studies demonstrated that the first contractile waves are due to spontaneous smooth muscle contractions (Chevalier, 2018; Roberts et al., 2010). The transition from uncoordinated to rhythmic motility patterns in the developing intestine has been associated with the activity of ENS (Chevalier et al., 2019; Roberts et al., 2010) and Interstitial Cells of Cajal (ICCs) (Chevalier et al., 2020), which are mesenchymal cells that have differentiated from digestive mesenchymal progenitors common to smooth muscle cells and ICCs (Lecoin et al., 1996; Young et al., 1996).

Therefore, a non-invasive *in vivo* approach that can reproducibly identify, quantify, and follow GI motility during fetal development is needed to identify the implicated physiological key mechanism(s) and monitor the emergence of motility. This will

allow scientists to understand how rhythmic motility patterns are set up and their alterations in infants with functional GI disorders (Martire et al., 2021; Thapar et al., 2018). Here, we used high-frequency ultrasound imaging and speckle tracking analysis to study GI motility in chick embryos. Compared with human/mouse embryos, the chick GI tract presents adaptive morphological differences (Smith et al., 2000). However, smooth muscle development and its colonization by ENS occur in the first third of the fetal period in human and chick embryos (Wallace and Burns, 2005; Faure et al., 2015; Bourret et al., 2017). Conversely, this colonization is not complete until the second third of development in mice (Heanue et al., 2016). Moreover, the main advantage of the chick embryo model is that it allows us to analyze directly by ultrasonography the digestive motility without being disturbed by the movement of the mother and without the use of anesthetics, which can influence the digestive motor activity (De Corte et al., 2012). With this method we could identify the *in vivo* early GI motility, its changes and functional profiles during chick embryo development. This approach combined with pharmacological inhibitors of smooth muscle contraction and of ENS or ICC activity allowed us to highlight ENS role in the stomach contraction synchronization *in vivo*. Moreover, by overexpressing the homeobox gene *BAPX1* in the stomach mesenchyme *in vivo*, we demonstrated that smooth muscle fiber organization is essential for functional fetal GI motility.

RESULTS

Stomach contraction undergoes dynamic changes to reach coordinated patterns during chick embryo development.

To enable the non-invasive *in vivo* investigation of the GI tract in chick embryos without need of anesthetics, we used the high-resolution echography imaging

technique that was previously applied to monitor heart changes during chick embryo development (McQuinn et al., 2007). At embryonic day 15 (E15), the latest stage we analyzed, we could visualize all embryonic GI segments (stomach, small intestine, and colon) and their associated organs (liver, lung, pancreas). Besides the anatomical structures, we also monitored the stomach deformations (Fig.1A, white arrows, dotted line) associated with the dynamic opening and closure of its lumen (Fig. 1A, red arrows and Movie 1). We observed these movements in small intestine and colon (Movies 2&3) as well. We then used high-resolution echography to investigate the onset and changes of stomach motility during embryogenesis, from E8 to E15. We started our analyses at E8 because the digestive tract expresses digestive smooth muscle differentiation markers at this stage (Faure et al., 2015, Notarnicola et al., 2012). We could visualize the stomach structure at E8, and unexpectedly, we observed stomach movements already at this stage (Fig. 1B, dotted line, Movie 4). After recording GI images for several minutes at 25 images/sec, we analyzed the GI tract movements in the part of the movies where the whole chick embryo did not move and used the speckle tracking analysis software (VevoLab) to analyze them. Strain was defined as the relative change in length, and was determined with the formula $\varepsilon = (L-L_0)/L_0$ where L_0 is the baseline length and L is the length at maximum contraction. Using this analysis, we generated a deformation map (3D strain) at E8 and quantified the stomach deformation (ranking from -9.5 to +10.3). We observed asynchronous deformations around the stomach circumference, suggesting that contractions began in an uncoordinated manner (Fig. 1C). At E13 (Fig. 1B, dotted line, Movie 5), the magnitude of stomach deformation increased (from -24.7 to +21.8), but became increasingly confined to specific zones (Fig. 1C). At E15 (Fig. 1B, dotted line), the stomach deformation percentage was still elevated (from -8.7 to

+21.9). Moreover, we observed that these deformations are regionalized (Fig. 1C), highlighting that stomach contraction evolves during development. Using high-resolution echography, we found that the stomach area increased rapidly (by 13-fold) between E8 and E15 (Figure 1D): from 2.33 ± 0.71 mm^2 at E8 to 21.41± 5.06 mm^2 at E13, and 30.47 ± 3.8 mm^2 at E15. To quantify stomach deformation changes between E8 and E15, we used the speckle-tracking strain curves obtained from high-resolution echography images. We quantified stomach motility asynchrony from the standard derivation of the maximum radial time-strain curves of the six gastric segments delineated in the developing stomach (Fig. 1E) and the time-strain curves generated for each segment by adapting a previously described synchrony index used to study peristalsis (Mittal et al., 2006). We found that asynchrony was very high at E8 (2092.58 ± 1068.62), decreased at E13 (930.79 ± 337.01), and was near the basal line (230.89 ± 172.28) at E15, indicating high movement synchronization at E15 (Fig. 1F). The asynchrony values at E13 and E15 were significantly different (Fig. 1F; $P<0.05$). Altogether, we demonstrated *in vivo* the stomach dynamic contraction pattern that changed to synchronized movements at E15.

During development, colon and stomach motility coordination patterns appear later than in small intestine.

Most previous studies on GI motility onset focused on the small intestine using organs isolated from mouse and chick embryos (Chevalier, 2018; Chevalier et al., 2020; Roberts et al., 2010). Using high-resolution echography, we could monitor the small intestine from E13 onwards, and we detected a rhythmic movement already at this stage (Fig. 2A, B, red arrows). The small intestine area increased from 0.196 ± 0.036 mm^2 at E13 to 0.406 ± 0.069 mm^2 at E15 (Fig. 2C; $P <0.05$). Using speckle tracking

analysis, we measured the circumferential and radial small intestine strains (i.e. change in length over the original length) (Fig. 2D). The absence of a significant difference in the percentages of small intestine circumferential (16.37% ± 3.04 at E13 and 16.89% ± 4.12 at E15) and radial (10.72% ± 2.74 at E13 and 11.88% ± 1.74 at E15) strains indicated no change in the small intestine contraction between E13 and E15 (Fig. 2E). We then observed the colon lumen in the longitudinal orientation, and detected dynamic movements with the presence of rhythmic waves (Fig. 2F, red arrows; Movie 3). The colon diameter slightly increased from 1.22 ± 0.24 mm at E13 to 1.34 ± 0.22 mm at E15 (Fig. 2H, not significant). Using speckle tracking analysis, we measured the colon longitudinal strain (Fig. 2G), and found that the longitudinal deformation was significantly increased at E15 compared with E13 (1.63 ± 0.78 at E13 and 4.35 ± 0.97 at E15) (Fig. 2H; $P < 0.05$). Altogether, we showed efficient small intestine motility already at E13, whereas the colon motor skills continued to progress from E13 to E15.

The enteric nervous system is implicated in fetal stomach contractions.

To challenge our high-resolution echography approach and to determine the origin of stomach contractions, we developed an approach to deliver in the GI lumen drugs that target specific cell types (smooth muscle cells, enteric neurons, and ICCs) found in the developing stomach musculature (Fig. 3A). As a prerequisite, Evans Blue solution directly deposited in the E15 chick embryo beak was observed 1 hour later in the stomach lumen (Fig. S1). Using high-resolution echography, we monitored stomach contractions at E15 before drug delivery and 1 hour after. As a control, we also determined the heart rate. We first evaluated the consequence of intra-oral saline solution (PBS) injection (negative control) and found that it did alter neither the GI

motility (velocity and radial displacement), nor the heart rate (Fig. S2A). Then, we used the inorganic calcium channel blocker cobalt chloride ($CoCl_2$) that blocks extracellular Ca2+ entry through L-type voltage-dependent Ca2+ channels and receptor-operated channels. $CoCl_2$ has been previously used to abolish the contraction of embryonic mouse and chick intestine in organ culture (Roberts et al., 2010; Chevalier et al., 2017). Using speckle tracking analysis, we measured the circumferential and radial stomach strains (i.e. change in length over the original length) (Fig. 3B). $CoCl_2$ led to a decrease in stomach circumferential velocity (from 6.51 ± 1.69 mm/sec before to 2.82 ± 0.46 mm/sec after treatment, $P < 0.05$) and radial displacement (from 0.169 ± 0.065 mm before to 0.082 ± 0.05 mm after treatment, $P < 0.05$) (Fig. 3C and S2B). Moreover, we confirmed that this approach specifically targets the stomach because the heart rate was not altered by $CoCl_2$ (185.6 ± 10.8 beats per minute (bpm) before and 188.8 ± 7.3 bpm after treatment, not significant) (Fig. 3C). These data demonstrated that the measured deformations were specific to the intrinsic stomach smooth muscle contractions. To evaluate ICC contribution to stomach contraction, we used imatinib to block ICC activity (Beckett et al., 2007; Chevalier et al., 2020; Kim et al., 2010; Popescu et al., 2006). After 1 hour, the stomach circumferential velocity (from 9.56 ± 1.04 mm/sec before to 3.03 ± 0.60 mm/sec after treatment, $P < 0.0001$) and radial displacement (from 0.237 ± 0.01 mm before to 0.064 ± 0.021 mm after treatment, $P < 0.001$) were decreased (Fig. S2C), leading to stomach contraction inhibition. As imatinib also affected the heart rate, which decreased from 212 ± 12 bpm before to 148.4 ± 24.7 bpm after treatment, ($P < 0.05$), we could not conclude regarding ICC role in stomach contraction regulation. We next used the sodium neural channel blocker tetrodotoxin (TTX) to evaluate ENS contribution (Roberts et al., 2010; Chevalier et al., 2017). We found that TTX

decreased the stomach circumferential velocity (from 7.46 ± 1.25 mm/sec before to 4.44 ± 1.88 mm/sec after treatment, P <0.05) and radial displacement (from 0.152 ± 0.058 mm before to 0.032 ± 0.010 mm after treatment, P <0.05) (Fig. 3D and S2D), leading to stomach contraction inhibition. The heart rate remained constant (180.8 ± 16.6 bpm before and 183.6 ± 10.7 bpm after treatment, not significant) (Fig. 3D). This data show that high-resolution echography can be used to monitor GI tract contractions *in vivo*, facilitating robust quantitative analysis. Moreover, using GI-targeted drug delivery, we found that at E15 the ENS contributes to stomach motility regulation.

Smooth muscle layer organization is essential for fetal stomach contraction coordination

The development of an approach to monitor digestive contractility *in vivo* opens the way to study the role of specific genes. BMP signaling activity is implicated in the development and differentiation of the digestive mesenchyme into smooth muscle (De Santa Barbara et al., 2005; Notarnicola et al., 2012). Upstream of the BMP ligand, *BAPX1* (also known as *NKX3.2*) is expressed in the vertebrate distal stomach mesenchyme (Faure et al., 2013; Nielsen et al., 2001; Verzi et al., 2009). As previously reported, *BAPX1* negatively regulates *BMP4* and *BMPRII* expression (Fig. S3A) and consequently BMP activity in the stomach mesenchyme (Fig. S3B), resulting in the expansion of the gastric and duodenal mesenchyme mass (De Santa Barbara et al., 2005; Nielsen et al., 2001) and in the increase of SMC proliferation (Fig. S3C). However, *BAPX1* functions in the stomach smooth muscle differentiation have not been investigated yet. Therefore, to evaluate the impact of BMP activity modulation on fetal stomach contractions, we used the avian replication-competent

retroviral misexpression system to continuously and specifically express *BAPX1* in the developing stomach mesenchyme (Fig. S3D), as previously described (Faure et al., 2015; McKey et al., 2016). High-resolution echography showed that the *BAPX1*-expressing stomach lumen of E13 chick embryos was devoid of refringent content compared with E13 *GFP*-expressing stomach lumens (controls) (Fig. 4A, compare white and yellow arrows). Moreover, *BAPX1*-expressing stomachs were hypotonic compared with controls and did not show a rhythmic muscular deformation and displacement (Movies 6 and 7). Using speckle tracking analysis, we found that the stomach circumferential velocity (5.734 ± 1.25 mm/sec in *BAPX1*-expressing and 8.202 ± 0.94 mm/sec in control stomachs, $P < 0.05$) and radial displacement (0.065 ± 0.025 mm in *BAPX1*-expressing and 0.1977 ± 0.054 mm in control stomachs, $P < 0.01$) (Figure 4B) were decreased in E13 *BAPX1*-expressing stomachs, leading to stomach contraction inhibition. We then evaluated *BAPX1* expression effect on the stomach morphology and smooth muscle differentiation status. *BAPX1* overexpression induced minor morphological defects in the distal and proximal stomach (respectively gizzard and proventriculus in birds) at E13 (Fig. 4C, upper panels). We confirmed the mesenchyme targeting by *BAPX1*- and *GFP*-expressing (control) retroviruses with anti-gag antibodies (Fig. 4C, lower panels; Fig. S3D). We detected the smooth muscle marker gamma smooth muscle actin (γSMA) by immunostaining in transversal paraffin sections of E13 control- and *BAPX1*-expressing stomachs, suggesting that the induction of contractile proteins in smooth muscle was not impaired (Fig. 4D and S3E). However, in *BAPX1*-expressing stomachs, the fiber structure was disorganized (Fig. 4D and S3E, compare white and red arrows). Expression of the pan-neuronal (B3-tubulin (TUJ1)) marker indicated that enteric neurons were present in both conditions (Fig. 4D and S3E). To better

characterize the smooth muscle organization, we modified and optimized the RapiClear® tissue-clearing protocol to obtain whole translucent stomachs. We assessed the 3D impact of *BAPX1* overexpression using light-sheet microscopy. In E13 control stomach samples, 3D analysis of γSMA expression highlighted the presence of several muscle bundles organized in parallel fibers with an orthogonal orientation in the most posterior part of the stomach (Fig. 4E, white arrow in the dorsal view; Movie 8). Like in control samples, in E13 *BAPX1*-expressing stomach samples, muscle bundles were organized in parallel fibers. However, the orthogonal orientation of the second muscle layer was altered: fibers were present, but harbored multiple orientations (Fig. 4E, red arrow in the ventral view; Movie 9). *BAPX1* expression also led to the inversion of the muscle bundle orientation (Fig. 4E, compare red and white arrows in the dorsal view). The changes in the muscle fiber orientation observed in whole *BAPX1*-expressing stomach samples were confirmed in virtual sections (Fig. 4F, compare red and white arrows). As intestinal smooth muscle differentiation contributes to ENS organization (Graham et al., 2017), we examined also the neuronal network. The ENS network spread in the smooth muscle layer sparing the tendons (Fig. 4E and 4F; Movie 8) (Le Guen et al., 2009). However, the neuronal mesh was less dense and less interconnected in E13 *BAPX1*-expressing stomachs where we observed disorganized smooth muscle bundles (Fig. 4E and 4F; Movie 9). Altogether, the combination of high-resolution echography *in vivo* imaging, gain of function approach, and 3D tissue-clearing immunofluorescence allowed us to demonstrate that BMP signaling deregulation in the stomach mesenchyme alters the segmental orientation of the smooth muscle layers, a feature associated with impaired fetal motility.

Discussion

Using an approach that combines *in vivo* non-invasive high-resolution echography imaging and speckle-tracking analysis, we characterized GI motility patterns during chick embryo development. We adapted and validated this approach that is mainly used in cardiovascular physiopathology for perinatal gastroenterology investigations using chick embryos, a vertebrate model that allows the longitudinal investigation of all GI domains.

Our *in vivo* approach allowed showing that the early erratic contractions of the stomach musculature observed at E8 became synchronized at E15. Investigation of other segments of the developing GI tract highlighted differences in motility onset along the AP axis. Like the stomach, the colon motility became fully efficient at E15. Conversely, the small intestine motility was effective at E13, as indicated by the presence of efficient waves of peristalsis. The timing of efficient intestinal motility coincides with the appearance of the longitudinal smooth muscle layer in the chick small intestine (Shyer et al., 2013), suggesting the requirement of the second smooth muscle layer for efficient contractions. The onset of GI smooth muscle differentiation and its regional differences have been previously described in the chick embryo (Bourret et al., 2017; Graham et al., 2017). Conversely, the precise timing of the sequential differentiation of the distinct smooth muscle layers along the AP of the GI tract was unknown. Our functional observations support regional differences in the appearance of the longitudinal smooth muscle layer.

Most of the GI variation among vertebrate species concerns the stomach morphology and can be correlated with their diverse diets. However, the global molecular patterning of the GI tract is remarkably similar among the different vertebrate

lineages (Smith et al., 2009). Stomach development and its specific morphogenesis have been extensively studied in several animal models (for review, (Grapin-Botton, 2005; Kim and Shivdasani, 2016; Le Guen et al., 2015; McLin et al., 2009)), but few studies have addressed the development of motor skills in organ culture, and even fewer *in vivo*. The human stomach musculature consists of two smooth muscle layers, an external longitudinal and internal circular muscle layer, for most of its extent. In addition, there is an oblique muscle layer, internal to the circular muscle layer, in the gastro-esophageal junction region (Di Natale et al., 2021; Hur, 2020). Adult gastric movements depend on the generation of electrical rhythmicity and electrical conduction. The directions and strengths of the forces generated when the muscle is excited, depend on the musculature organization. However, there is no detailed quantitative data on the vertebrate stomach musculature organization, although their innervation has been extensively described (Furness et al., 2020). Using the high-resolution echography/speckle tracking approach and pharmacological inhibitors, we found that stomach contractions are controlled by enteric neurons at E15. This suggests the importance of the establishment of stomach contraction to ensure the fetal transit that is also essential for the fetus growth. Using a genetic approach, we then showed that deregulation of the BMP pathway activity affects the organization of the longitudinal smooth muscle layer and its orientation relative to the circular layer, but not gastric smooth muscle differentiation and the oblique smooth muscle layer. The high-resolution echography/speckle tracking approach in *BAPX1*-expressing embryos allowed us to detect *in vivo* a functional alteration that impaired contraction, despite the effective smooth muscle cell differentiation, highlighting the importance of this new approach.

Our data demonstrated differences in peristalsis onset along the AP axis at a developmental stage that in the human embryo corresponds to 12 and 14 weeks of gestation. The pediatric Chronic Intestinal Pseudo-Obstruction (CIPO) syndrome is the most severe functional gastrointestinal disorder (high morbidity and mortality rates), but lacks standardized diagnostic and therapeutic approaches (Thapar et al., 2018). Recently, it was reported that the *ACTG2* gene, which encodes γSMA, is mutated in 30% of children with CIPO who have a worse outcomes and severe GI dysmotility often associated with the presence of megacystis (Hashmi et al., 2021; Matera et al., 2016). In pediatric patients with CIPO, prenatal signs are detected only in about 20% of cases, mainly the presence of megacystis, although 50–70% of affected infants show clinical signs in the first month after birth (Di Nardo et al., 2017). Multi-visceral dilation has been observed, using standard ultrasonography, in two fetuses with CIPO (Shen et al., 2007). This suggests that the non-invasive high-resolution echography approach could be useful to easily and routinely assess digestive function in fetuses before birth. However, routine ultrasound examination to detect GI dysmotility is not part of the recent antenatal recommendations (Thapar et al., 2018).

Altogether, we demonstrated that GI contractions occur during fetal development and progress from an uncoordinated pattern to a more powerful coordinated profile, showing that the intrinsic extrinsic innervation influence embryonic peristalsis.

MATERIALS AND METHODS

Animal model and ultrasound data acquisition and analysis

Fertilized white Leghorn chicken eggs (Les Bruyères, Dangers, France) were incubated at 38°C in a humidified incubator (SMA Coudelou, France) until use.

Although experiments using chick embryos do not require approval by an ethic committee (European law, article 2016/63/UE), they were performed in accordance with the INSERM and CNRS ethics guidelines for animal experimentation. After 2 days of incubation, 4 ml of albumin was removed and a hole was made and sealed with tape to avoid the formation of vessels on the shell top. Briefly, eggs were taken out of the incubator and held under a bright light to localize the embryo. Then, a window of approximately 1.5 by 1.5 cm was sawn in the eggshell. The eggshell and outer membrane were removed to visualize the embryo that was staged by microscopic examination according to Hamburger and Hamilton (Hamburger and Hamilton, 1951) and Southwell (Southwell, 2006). Embryos that were dysmorphic or showed visible bleeding were excluded. E8 (stage 34), E13 (stage 39), and E15 (stage 41) embryos were studied *in vivo* (n=6 embryos per stage). At these stages, embryos float on the left side in the egg yolk. During ultrasonography, each egg was positioned in a dry block heater filled with sand to maintain the temperature of 38°C inside the egg. The Vevo2100 and Vevo3100 (Visualsonics) ultrasound systems with 40 MHz probes (MS550D and MX550D) were used for *in vivo* image acquisition (spatial resolution of 40 µm). Briefly, the probe was delicately positioned on the eggshell window using an adjustable stand and transducer mount. B-Mode was used to record 2D images of the GI tract for 1 minute at 25 images/sec. As ultrasound image acquisition of the embryos was performed without anesthesia, the embryo could move in its shell. For this reason, movies were recorded for several minutes, but the movements of the GI tract were analyzed using only the movie parts where the embryo was not moving. For the small intestine evaluation, 3-5 movie parts per embryo were analyzed to obtain a mean value for minimizing size variability. B-mode videos were transferred to ImageJ to measure the cross-sectional area and diameter.

The speckle tracking analysis software (VevoLab 5.6.1) was used off-line to analyze the GI tissue motion by tracking natural acoustic reflection interference, also called speckle pattern. The speckle tracking algorithm used in this study allows us to calculate and to quantify the maximum regional (stomach, intestine and colon) velocity, displacement, and strain from E8 to E15. Strain is defined as the relative change in length, and is determined with the formula $\varepsilon = (L-L_0)/L_0$ where L_0 is the baseline length and L is the length at maximum contraction. The circumferential strain, radial strain and longitudinal strain identify the contraction along the circular outline, the organ thickening, and the length change relative to the original organ length, respectively. It should be noted that our strain values are likely to be underestimated due to the use of Lagrangian linear methods. Statistical analyses were done with the Prism 8 software and one-way ANOVA with Tukey's multiple comparison test and a single pool of variance.

Pharmacological inhibition

To delivery specific compounds in the GI tract, an intra-oral administration technique was developed. To allow the access to the beak of E15 embryos, a high temperature cautery handle (Bovie Medical Corporation, FST) was used to open a small window without bleeding into the extraembryonic membranes close to the beak. To validate this approach, Evans Blue solution was deposited directly in the E15 chick embryo beak with a capillary pipette and 1 hour later the dye was detected in the stomach lumen (Fig. S1). The sodium channel blocker TTX (1 mM stock solution, Tocris, Bristol, UK) was used to block neurotransmission (D'Antona et al., 2001), and the calcium channel blocker $CoCl_2$ (0.1 M stock solution, Sigma-Aldrich, France) was used to block smooth muscle contraction (de Moraes and Carvalho, 1969). Imatinib

mesylate (STI571) (10 mM stock solution, Euromedex, France) was used to block the receptor tyrosine kinase protein KIT and ICC activity (Beckett et al., 2007; Chevalier et al., 2020). Drugs were diluted to the final concentration by adding sterile PBS. Before drug administration, the stomach and heart of each E15 embryo were evaluated by high-resolution echography. This was followed by intra-oral administration of 100 µl of 25 µM TTX, 100 µl of 10 µM $CoCl_2$, 100 µl of 20 µM imatinib, or 100 µl of PBS (control). To determine TTX optimal concentration that leads to reproducible stomach motility inhibition without any effect on heart rate (i.e. 25 µM), 1, 10, 25 and 50 µM were tested in preliminary experiments. Using fine tools and syringes, the solution was dropped in the beak, and each egg was put back in the incubator to allow the drug progression to the GI tract. After 1 hour, each egg was evaluated by high-resolution echography, as previously described. Following this protocol, we also evaluated and found that intra-oral administration of PBS alone did not affect GI motility compared with untreated E15 embryos (Fig. S2A). Five embryos per stage were studied without exclusion criteria. The paired *t*-test was calculated with the Prism 8 software.

Avian retroviral misexpression system, RapiClear® tissue clearing, and light-sheet microscopy analysis

Fertilized White Leghorn eggs were incubated at 38°C in humidified incubators. The vector to produce replication-competent retroviruses (RCAS) was previously described (Le Guen et al., 2009; Moniot et al., 2004). The DF-1 chicken fibroblast cell line (ATCC-LGC) was transfected with RCAS-based constructs to produce retroviruses that express GFP (Moniot et al., 2004) or BAPX1 (De Santa Barbara et al., 2005; Nielsen et al., 2001). *GFP*-expressing retroviruses alone (as control) or a

mix of *BAPX1+GFP*-expressing retroviruses were injected in the splanchnopleural mesoderm of stage 10 chick embryos to target the stomach mesenchyme (Le Guen et al., 2009; Moniot et al., 2004; Notarnicola et al., 2012; Roberts et al., 1998). This direct splanchnopleural mesoderm injection and the specific trophism of retroviruses for mesenchymal cells prevent the targeting of vENCDCs and epithelium ((Faure et al., 2015); Fig. S3D). Eggs were then placed at 38°C until high-resolution echography followed by dissection. Only GFP-positive stomachs were analyzed by high-resolution echography and underwent RapiClear® tissue clearing.

For immunofluorescence of paraffin sections, stomachs were gradually dehydrated in ethanol and embedded in paraffin; 10-µm sections were cut using a microtome and collected on poly-L-lysine-coated slides (Thermo Fisher) for immunofluorescence (Faure et al., 2013) using rabbit anti-γSMA (MyBioSource, MBS820899, 1:500 dilution), using rabbit phospho-histone H3-Ser10 (PH3) (Millipore, 1:500 dilution) and mouse anti-TUJ1 (Covance, 1:800 dilution) antibodies. Nuclei were stained with Hoechst 33342 (Molecular Probes). Cells were imaged with a Zeiss AxioVision fluorescence microscope using standard filters, or a ZEISS LSM800 confocal laser-scanning microscope.

For tissue clearing, GI tissues were fixed at room temperature (RT) on an orbital shaker in 4% paraformaldehyde for 2 hours, and then washed in PBS for 1 hour. Samples were transferred to 2% Triton X-100 in PBS solution (containing 0.05% sodium azide) for permeabilization at RT on an orbital shaker for 1-2 days, and then washed 3 times for 15min in PBS at RT. Samples were incubated at 4°C on an orbital shaker in blocking solution (10% normal donkey serum, 1% Triton-X100, 0.2% sodium azide in PBS) for 2 days, followed by incubation with primary antibodies (rabbit anti-γSMA (1:300 dilution, and mouse anti-TUJ1, Covance, 1:200 dilution) in

antibody dilution buffer (1% normal donkey serum, 0.2% Triton-X100, 0.2% sodium azide in PBS) at 4°C on an orbital shaker for 3-4 days. Then, samples were washed with washing buffer (3% NaCl, 0.2% Triton-X100 in PBS) on an orbital shaker 3 times at RT for 1 hour, and then at 4°C overnight. Samples were incubated with the anti-rabbit Alexa Fluor 647 (A31573 Invitrogen, 1:300 dilution) and anti-mouse Alexa Fluor 568 (A10037 Invitrogen, 1:300 dilution) secondary antibodies, in dilution buffer at 4°C on an orbital shaker for 2 days. Samples were washed with washing buffer on an orbital shaker at RT 3 times for 1 hour and then at 4°C overnight. This was followed by three washes with PBS for 15 minutes/each and sample clearing with RapiClear® at RT overnight. Cleared specimens were placed in 2,2'-Thiodiethanol solution (#166782 Sigma) and tissues were imaged using light-sheet microscopy (UltraMicroscope Blaze, Miltenyi Lavision BioTec), a 2X objective (MVPLAPO Olympus) and 0.5X numerical aperture. Images were analyzed with Imaris.

Author Contributions

P.S., S.F., J.T., N.C. and P.d.S.B. conceived the study and designed the experiments. P.S., S.F., S.E.L., A.F., and N.C. performed the experiments. P.S., and P.d.S.B. analyzed the results. All authors contributed to the writing and approved the final manuscript.

Acknowledgments

The authors thank the members of the "Development of visceral smooth muscle and associated pathologies" team (PhyMedExp), Patrice Bideaux for technical assistance, Emilie Josse for graphical art, the Imagerie du Petit Animal de Montpellier (IPAM, Biocampus Montpellier) for access to high-resolution ultrasound (LRQA Iso9001;

France Life Imaging (grant ANR-11-INBS-0006); IBISA; Fondation Leducq (Grant RETP), I-Site Muse) and Montpellier Ressources Imagerie for access to light-sheet microscopy (M-P. Blanchard, A. Sarrazin and O. Faklaris, MRI, Biocampus, Montpellier) facilities.

Funding

This work was supported by the French Patients' Association POIC, FIMATHO (2021), Agence Nationale de la Recherche ANR-17-CE14-0043 (PAPIS) to P.d.S.B., and the Association Française contre les Myopathies (AFM) (No 23800) and ANR-21-CE14-0017 (NeuroPIMM) to S.F.

REFERENCES

Barnes, K. J., Beckett, E. A., Brookes, S. J., Sia, T. C. and Spencer, N. J. (2014). Control of intrinsic pacemaker frequency and velocity of colonic migrating motor complexes in mouse. *Front Neurosci* **8**, 96.

Beckett, E. A. H., Ro, S., Bayguinov, Y., Sanders, K. M. and Ward, S. M. (2007). Kit signaling is essential for development and maintenance of interstitial cells of Cajal and electrical rhythmicity in the embryonic gastrointestinal tract. *Dev Dyn* **236**, 60–72.

Bourret, A., Chauvet, N., de Santa Barbara, P. and Faure, S. (2017). Colonic mesenchyme differentiates into smooth muscle before its colonization by vagal enteric neural crest-derived cells in the chick embryo. *Cell Tissue Res* **368**, 503–511.

Burns, A. J. and Douarin, N. M. (1998). The sacral neural crest contributes neurons and glia to the post-umbilical gut: spatiotemporal analysis of the development of the enteric nervous system. *Development* **125**, 4335–4347.

Burns, A. J., Champeval, D. and Le Douarin, N. M. (2000). Sacral neural crest cells colonise aganglionic hindgut in vivo but fail to compensate for lack of enteric ganglia. *Dev Biol* **219**, 30–43.

Burns, A. J., Roberts, R. R., Bornstein, J. C. and Young, H. M. (2009). Development of the enteric nervous system and its role in intestinal motility during fetal and early postnatal stages. *Semin Pediatr Surg* **18**, 196–205.

Chevalier, N. R., Fleury V., Dufour, S., Proux-Gillardeaux V., Asnacios, A. (2017). Emergence and development of gut motility in the chicken embryo. *PLoS One* 12, e0172511.

Chevalier, N. R. (2018). The first digestive movements in the embryo are mediated by mechanosensitive smooth muscle calcium waves. *Philos Trans R Soc Lond B Biol Sci* **373**, 20170322.

Chevalier, N. R., Dacher, N., Jacques, C., Langlois, L., Guedj, C. and Faklaris, O. (2019). Embryogenesis of the peristaltic reflex. *J Physiol* **597**, 2785–2801.

Chevalier, N. R., Ammouche, Y., Gomis, A., Teyssaire, C., de Santa Barbara, P. and Faure, S. (2020). Shifting into high gear: how interstitial cells of Cajal change the motility pattern of the developing intestine. *Am J Physiol Gastrointest Liver Physiol* **319**, G519–G528.
D'Antona, G., Hennig, G. W., Costa, M., Humphreys, C. M. and Brookes, S. J. (2001). Analysis of motor patterns in the isolated guinea-pig large intestine by spatio-temporal maps. *Neurogastroenterol Motil* **13**, 483–492.
De Corte, W., Delrue, H., Vanfleteren, L. J., Dutré, P. E., Pottel, H., Devriendt, D. K., Van Rooy, F. H., D'Hondt, M., Carlier, S. and Desmet, M. B. (2012). Randomized clinical trial on the influence of anaesthesia protocol on intestinal motility during laparoscopic surgery requiring small bowel anastomosis. *Br J Surg* **99**, 1524-1529.
de Moraes, S. and Carvalho, F. V. (1969). Cobalt ion and the mechanical response of the depolarized smooth muscle. *Pharmacology* **2**, 230–236.
de Santa Barbara, P., van den Brink, G. R. and Roberts, D. J. (2002). Molecular etiology of gut malformations and diseases. *Am. J. Med. Genet.* **115**, 221–230.
de Santa Barbara, P., van den Brink, G. R. and Roberts, D. J. (2003). Development and differentiation of the intestinal epithelium. *Cell Mol Life Sci* **60**, 1322–1332.
De Santa Barbara, P., Williams, J., Goldstein, A. M., Doyle, A. M., Nielsen, C., Winfield, S., Faure, S. and Roberts, D. J. (2005). Bone morphogenetic protein signaling pathway plays multiple roles during gastrointestinal tract development. *Dev. Dyn.* **234**, 312–322.
Di Nardo, G., Di Lorenzo, C., Lauro, A., Stanghellini, V., Thapar, N., Karunaratne, T. B., Volta, U. and De Giorgio, R. (2017). Chronic intestinal pseudo-obstruction in children and adults: diagnosis and therapeutic options. *Neurogastroenterol Motil* **29**, e12956.
Di Natale, M. R., Patten, L., Molero, J. C., Stebbing, M. J., Hunne, B., Wang, X., Liu, Z. and Furness, J. B. (2022). Organisation of the musculature of the rat stomach. *J Anat* **240,** 711-723.
Fairman, C. L., Clagett-Dame, M., Lennon, V. A. and Epstein, M. L. (1995). Appearance of neurons in the developing chick gut. *Dev Dyn* **204**, 192–201.
Faure, S., Georges, M., McKey, J., Sagnol, S. and de Santa Barbara, P. (2013). Expression pattern of the homeotic gene Bapx1 during early chick gastrointestinal tract development. *Gene Expr Patterns* **13**, 287–292.
Faure, S., McKey, J., Sagnol, S. and de Santa Barbara, P. (2015). Enteric neural crest cells regulate vertebrate stomach patterning and differentiation. *Development* **142**, 331–342.
Furness, J. B., Di Natale, M., Hunne, B., Oparija-Rogenmozere, L., Ward, S. M., Sasse, K. C., Powley, T. L., Stebbing, M. J., Jaffey, D. and Fothergill, L. J. (2020). The identification of neuronal control pathways supplying effector tissues in the stomach. *Cell Tissue Res* **382**, 433–445.
Graham, H. K., Maina, I., Goldstein, A. M. and Nagy, N. (2017). Intestinal smooth muscle is required for patterning the enteric nervous system. *J Anat* **230**, 567–574.
Grapin-Botton, A. (2005). Antero-posterior patterning of the vertebrate digestive tract: 40 years after Nicole Le Douarin's PhD thesis. *Int J Dev Biol* **49**, 335–347.
Hamburger, V. and Hamilton, H. L. (1951). A series of normal stages in the development of the chick embryo. *J Morphol* **88**, 49–92.

Hashmi, S. K., Ceron, R. H. and Heuckeroth, R. O. (2021). Visceral myopathy: clinical syndromes, genetics, pathophysiology, and fall of the cytoskeleton. *Am J Physiol Gastrointest Liver Physiol* **320**, G919–G935.
Heanue, T. A., Shepherd, I. T. and Burns, A. J. (2016). Enteric nervous system development in avian and zebrafish models. *Dev Biol* **417**, 129–138.
Hur, M.-S. (2020). Muscular Architecture of the Abdominal Part of the Esophagus and the Stomach. *Clin Anat* **33**, 530–537.
Huycke, T. R., Miller, B. M., Gill, H. K., Nerurkar, N. L., Sprinzak, D., Mahadevan, L. and Tabin, C. J. (2019). Genetic and Mechanical Regulation of Intestinal Smooth Muscle Development. *Cell* **179**, 90-105.e21.
Kim, T.-H. and Shivdasani, R. A. (2016). Stomach development, stem cells and disease. *Development* **143**, 554–565.
Kim, B. J., Chae, H., Kwon, Y. K., Choi, S., Jun, J. Y., Jeon, J.-H., So, I. and Kim, S. J. (2010). Effects of imatinib mesylate in interstitial cells of Cajal from murine small intestine. *Biol Pharm Bull* **33**, 993–997.
Koppen, I. J. N., Benninga, M. A. and Singendonk, M. M. J. (2017). Motility disorders in infants. *Early Hum Dev* **114**, 1–6.
Lecoin, L., Gabella, G. and Le Douarin, N. (1996). Origin of the c-kit-positive interstitial cells in the avian bowel. *Development* **122,** 725-733.
Le Douarin, N. M. and Teillet, M. A. (1973). The migration of neural crest cells to the wall of the digestive tract in avian embryo. *J Embryol Exp Morphol* **30**, 31–48.
Le Guen, L., Notarnicola, C. and de Santa Barbara, P. (2009). Intermuscular tendons are essential for the development of vertebrate stomach. *Development* **136**, 791–801.
Le Guen, L., Marchal, S., Faure, S. and de Santa Barbara, P. (2015). Mesenchymal-epithelial interactions during digestive tract development and epithelial stem cell regeneration. *Cell. Mol. Life Sci.* **72**, 3883–3896.
Martire, D., Garnier, S., Sagnol, S., Bourret, A., Marchal, S., Chauvet, N., Guérin, A., Forgues, D., Berrebi, D., Chardot, C., et al. (2021). Phenotypic switch of smooth muscle cells in paediatric chronic intestinal pseudo-obstruction syndrome. *J Cell Mol Med* **25**, 4028–4039.
Matera, I., Rusmini, M., Guo, Y., Lerone, M., Li, J., Zhang, J., Di Duca, M., Nozza, P., Mosconi, M., Pini Prato, A., et al. (2016). Variants of the ACTG2 gene correlate with degree of severity and presence of megacystis in chronic intestinal pseudo-obstruction. *Eur J Hum Genet* **24**, 1211–1215.
McKey, J., Martire, D., de Santa Barbara, P. and Faure, S. (2016). LIX1 regulates YAP1 activity and controls the proliferation and differentiation of stomach mesenchymal progenitors. *BMC Biol.* **14**, 34.
Mclain, C. R. (1963). Amniography studies of the gastrointestinal motility of the human fetus. *Am J Obstet Gynecol* **86**, 1079–1087.
McLin, V. A., Henning, S. J. and Jamrich, M. (2009). The role of the visceral mesoderm in the development of the gastrointestinal tract. *Gastroenterology* **136**, 2074–2091.
McQuinn, T. C., Bratoeva, M., Dealmeida, A., Remond, M., Thompson, R. P. and Sedmera, D. (2007). High-frequency ultrasonographic imaging of avian cardiovascular development. *Dev Dyn* **236**, 3503–3513.
Mittal, R. K., Padda, B., Bhalla, V., Bhargava, V., Liu, J. (2006). Synchrony between circular and longitudinal muscle contractions during peristalsis in normal subjects. *Am J Physiol Gastrointest Liver Physiol* **290,** G431-438.

Moniot, B., Biau, S., Faure, S., Nielsen, C. M., Berta, P., Roberts, D. J. and de Santa Barbara, P. (2004). SOX9 specifies the pyloric sphincter epithelium through mesenchymal-epithelial signals. *Development* **131**, 3795–3804.
Nielsen, C., Murtaugh, L. C., Chyung, J. C., Lassar, A. and Roberts, D. J. (2001). Gizzard formation and the role of Bapx1. *Dev Biol* **231**, 164–174.
Notarnicola, C., Rouleau, C., Le Guen, L., Virsolvy, A., Richard, S., Faure, S. and De Santa Barbara, P. (2012). The RNA-binding protein RBPMS2 regulates development of gastrointestinal smooth muscle. *Gastroenterology* **143**, 687-697.e9.
Popescu, L. M., Vidulescu, C., Curici, A., Caravia, L., Simionescu, A. A., Ciontea, S. M. and Simion, S. (2006). Imatinib inhibits spontaneous rhythmic contractions of human uterus and intestine. *Eur J Pharmacol* **546**, 177–181.
Roberts, D. J. (2000). Molecular mechanisms of development of the gastrointestinal tract. *Dev Dyn* **219**, 109–120.
Roberts, D. J., Smith, D. M., Goff, D. J. and Tabin, C. J. (1998). Epithelial-mesenchymal signaling during the regionalization of the chick gut. *Development* **125**, 2791–2801.
Roberts, R. R., Ellis, M., Gwynne, R. M., Bergner, A. J., Lewis, M. D., Beckett, E. A., Bornstein, J. C. and Young, H. M. (2010). The first intestinal motility patterns in fetal mice are not mediated by neurons or interstitial cells of Cajal. *J Physiol* **588**, 1153–1169.
Sase, M., Tamura, H., Ueda, K. and Kato, H. (1999). Sonographic evaluation of antepartum development of fetal gastric motility. *Ultrasound Obstet Gynecol* **13,** 323–326.
Shen, O., Schimmel, M. S., Eitan, R., Granovsky-Grisaru, S. and Rabinowitz, R. R. (2007). Prenatal diagnosis of intestinal pseudo-obstruction. *Ultrasound Obstet Gynecol* **29**, 229–231.
Shyer, A. E., Tallinen, T., Nerurkar, N. L., Wei, Z., Gil, E. S., Kaplan, D. L., Tabin, C. J. and Mahadevan, L. (2013). Villification: how the gut gets its villi. *Science* **342**, 212–218.
Singendonk, M. M. J., Rommel, N., Omari, T. I., Benninga, M. A. and van Wijk, M. P. (2014). Upper gastrointestinal motility: prenatal development and problems in infancy. *Nat Rev Gastroenterol Hepatol* **11**, 545–555.
Smith, D. M., Grasty, R. C., Theodosiou, N. A., Tabin, C. J. and Nascone-Yoder, N. M. (2000). Evolutionary relationships between the amphibian, avian, and mammalian stomachs. *Evol Dev* **2**, 348-359.
Southwell, B. R. (2006). Staging of intestinal development in the chick embryo. *Anat Rec A Discov Mol Cell Evol Biol* **288**, 909–920.
Thapar, N., Saliakellis, E., Benninga, M. A., Borrelli, O., Curry, J., Faure, C., De Giorgio, R., Gupte, G., Knowles, C. H., Staiano, A., et al. (2018). Paediatric Intestinal Pseudo-obstruction: Evidence and Consensus-based Recommendations From an ESPGHAN-Led Expert Group. *J Pediatr Gastroenterol Nutr* **66**, 991–1019.
Uesaka, T., Young, H. M., Pachnis, V., and Enomoto, H. (2016). Development of the intrinsic and extrinsic innervation of the gut. *Dev Biol* **417,** 158-167.
Verzi, M. P., Stanfel, M. N., Moses, K. A., Kim, B.-M., Zhang, Y., Schwartz, R. J., Shivdasani, R. A. and Zimmer, W. E. (2009). Role of the homeodomain transcription factor Bapx1 in mouse distal stomach development. *Gastroenterology* **136**, 1701–1710.

Wallace, A.S. and Burns, A.J. (2005). Development of the enteric nervous system, smooth muscle and interstitial cells of Cajal in the human gastrointestinal tract. *Cell Tissue Res* **319**, 367-382.
Yntema, C. L. and Hammond, W. S. (1954). The origin of intrinsic ganglia of trunk viscera from vagal neural crest in the chick embryo. *J Comp Neurol* **101**, 515–541.
Young, H.M., Ciampoli, D., Southwell, B.R. and Newgreen, D.F. (1996). Origin of interstitial cells of Cajal in the mouse intestine. *Dev Biol* **180,** 97-107.

Figures

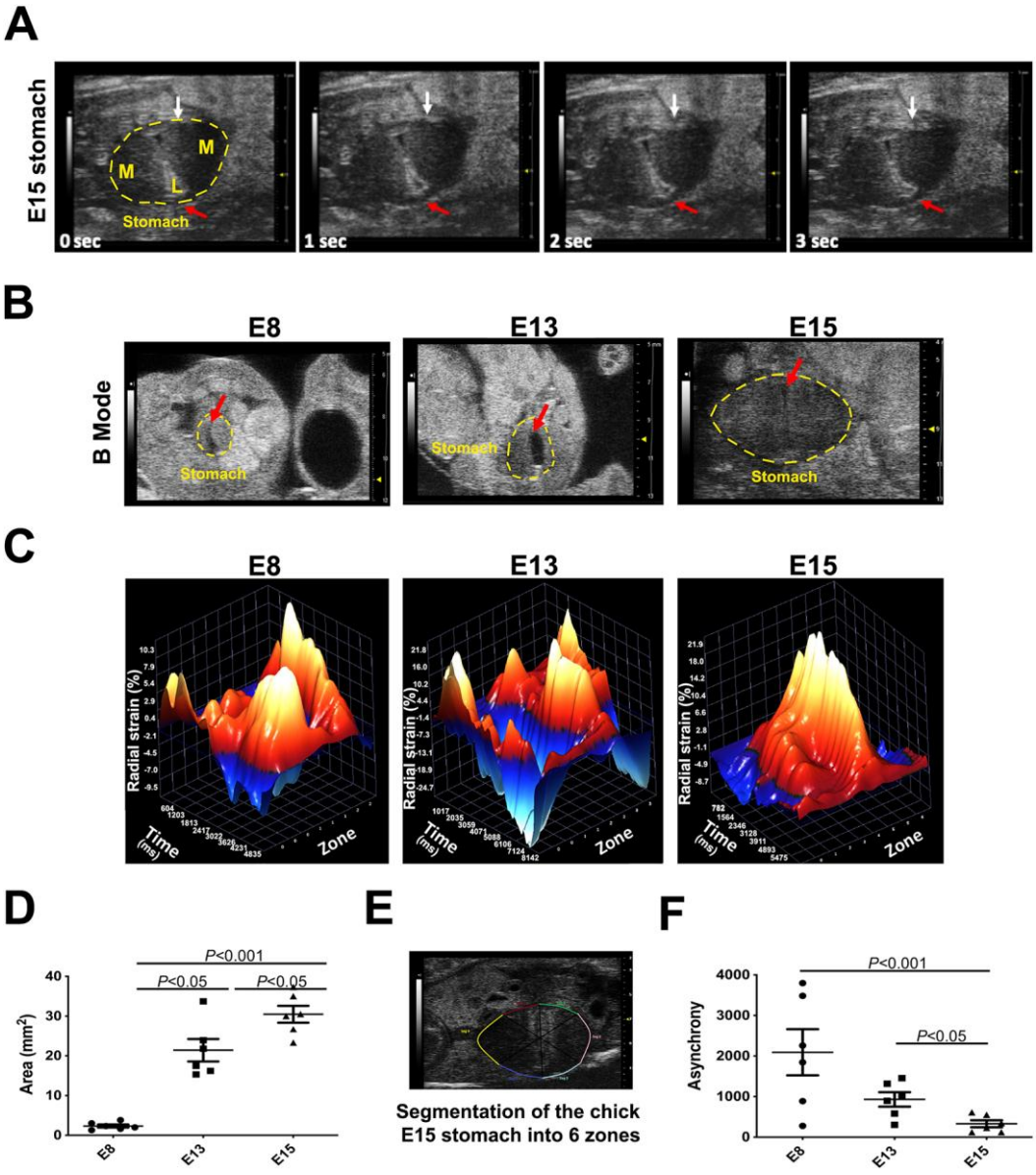

Fig. 1: Dynamic contractile activity during fetal chick stomach development. (A) Observation of stomach contractions *in vivo* using high-resolution echography in E15 chick embryos. Dotted line, E15 stomach; white arrows, muscle contraction waves; red arrows, lumen movement. (B) Stomach anatomy *in vivo* analysis using high-resolution echography at different stages of chick embryo development (E8, E13, and E15). Dotted lines, E8, E13 and E15 stomach; red arrows, stomach lumen. (C) 3D strain representation of the stomach contractile activity *in vivo* using high-resolution

echography imaging data during chick embryo development (E8, E13, and E15). 3D heat map of the radial strain percentage (z) for each individual stomach segment (y) during 5-8 sec of acquisition (x). (D) Quantification of the stomach area at the indicated developmental stages (n=6/stage). (E) Segmentation of the chick embryo stomach into six zones to monitor deformation. (F) Evaluation of asynchrony at the indicated developmental stages (n=6/stage).

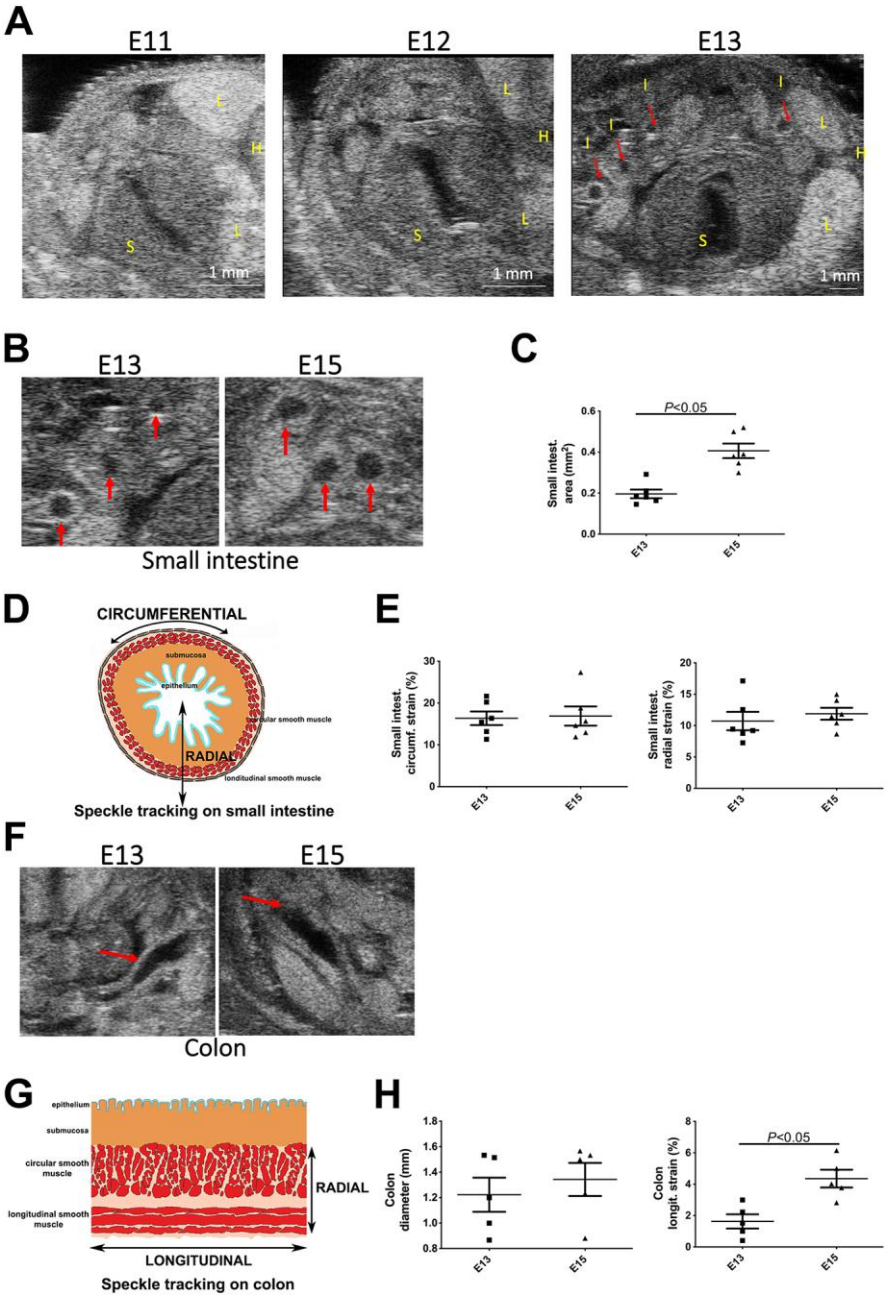

Fig. 2: Dynamic contractile activity during chick embryo small intestine and colon development. (A) Small intestine anatomy *in vivo* using high-resolution echography during chick embryo development: E11 (stage 37), E12 (stage 38), and E13 (stage 39). Red arrows, small intestine lumen. Abbreviations: H, heart; I, small intestine; L: lung; S, stomach. (B) Small intestine anatomy by high-resolution echography at E13 and E15. Red arrows, small intestine lumen. (C) Quantification of the small intestine area at the indicated developmental stages (n=6/stage). (D) Schematic representation of the speckle tracking analysis of the small intestine during chick embryo development. (D) Quantification of small intestine circumferential and

radial strains at the indicated developmental stages (n=6/stage). (F) Colon anatomy analysis by high-resolution echography at E13 and E15. Red arrows, colon lumen. (G) Schematic representation of the speckle tracking analysis of colon during chick embryo development. (H) Quantification of colon diameter and longitudinal strain at the indicated developmental stages (n=5/stage).

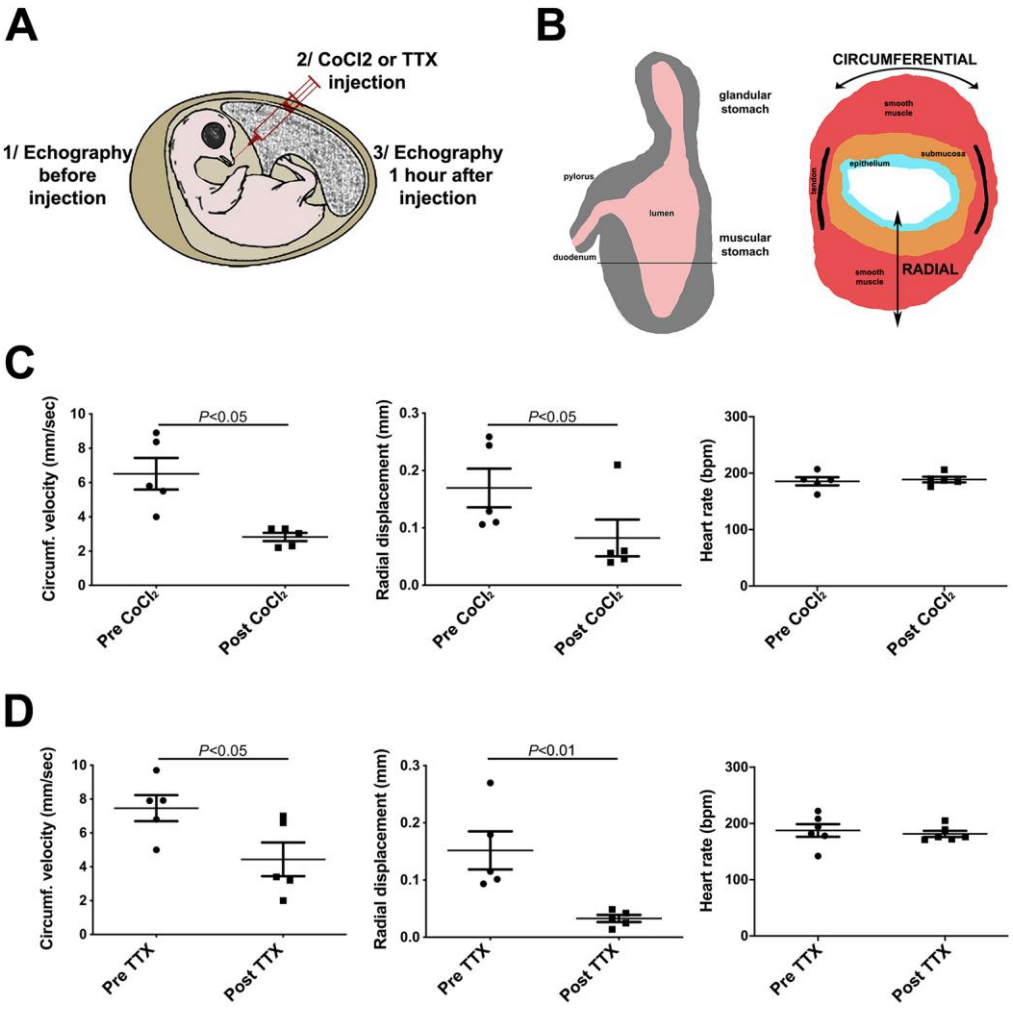

Fig. 3: Monitoring stomach contractile activity in E15 chick stomach. (A) Schematic representation of the method used to target the GI tract with drugs. (B) Schematic representation of the speckle tracking analysis of stomach during chick embryo development. (C) Effect of cobalt chloride (10 µM; $CoCl_2$) on stomach circumferential strain velocity, stomach radial strain changes, and heart rate in E15 chick embryos (n=5). (D) Effect of tetrodotoxin (25 µM; TTX) on stomach circumferential strain velocity, stomach radial strain changes, and heart rate in E15 embryos (n=5).

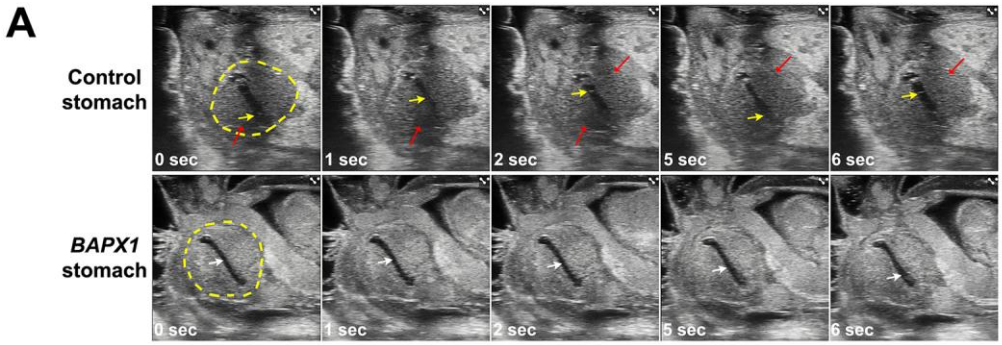

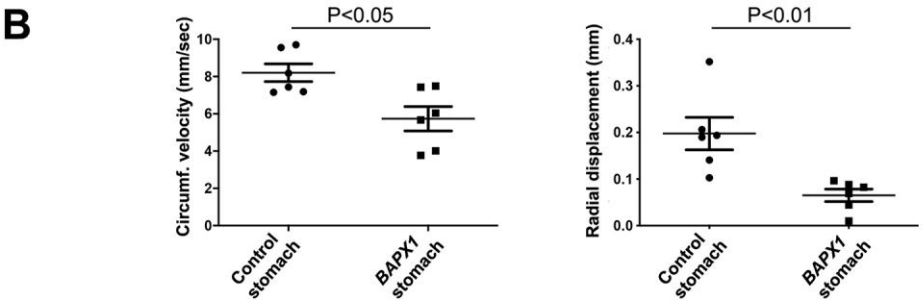

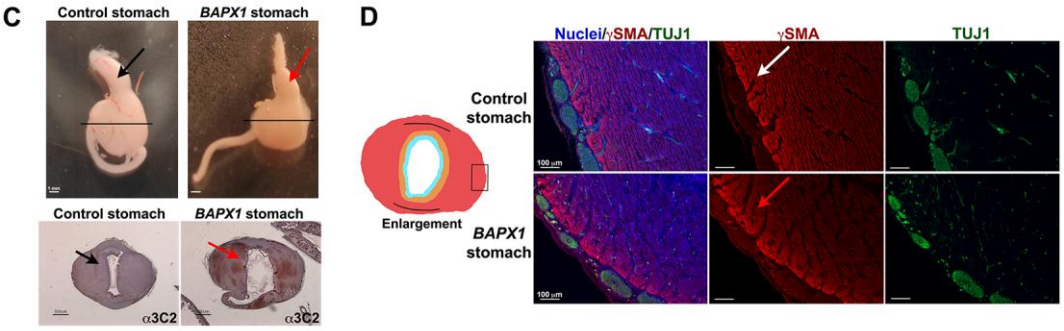

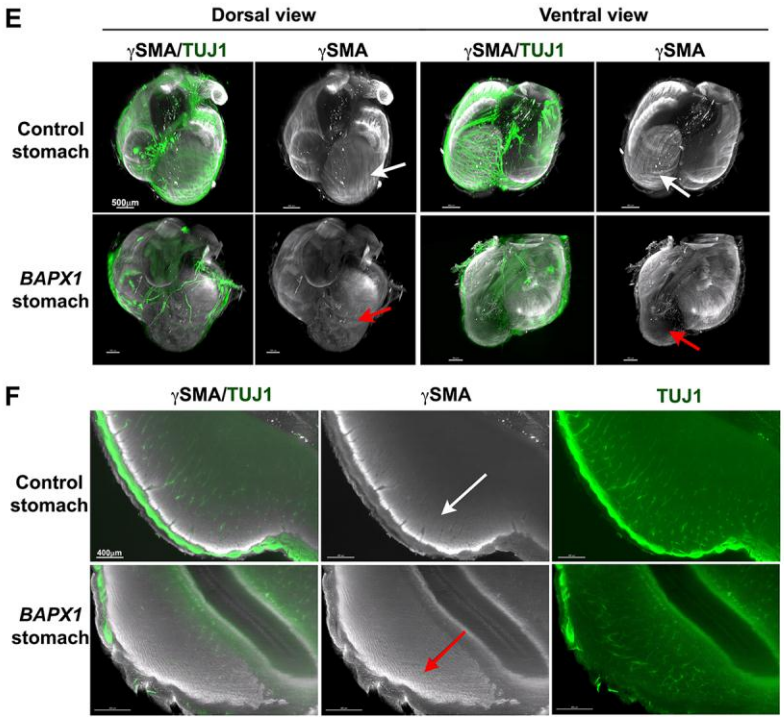

Fig. 4: Interfering *in vivo* with the BMP signaling pathway affects stomach contractility in chick embryos. (A) Observation of stomach contractions *in vivo* using high-resolution echography in E13 Control and *BAPX1*-overexpressing stomachs. Dotted line, E13 stomach; yellow arrows, refringent content (food) in the E13 control stomach lumen; white arrows, absence of refringent content (food) in *BAPX1*-overexpressing stomach lumen; red arrows, muscle movement in the control E13 stomach. (B) Speckle tracking analysis to evaluate the impact of BAPX1 expression on stomach circumferential strain velocity and radial strain changes in E13 chick embryos (n=6). (C) Effect of BAPX1 expression on E13 *BAPX1*-expressing stomach gross morphology compared with Control E13 stomach (upper panels; ventral view). Red and black arrows indicate the resulting proventriculus. Transversal paraffin sections of E13 Control and *BAPX1*-expressing stomachs analyzed by immunohistochemistry with an anti-gag (3C2) antibody (lower panel). Red arrows indicate *BAPX1* expression in the E13 *BAPX1*-expressing stomach. Scale bars: 500μm. (D) Transversal paraffin sections of E13 *BAPX1*-expressing and Control stomachs located in the external part of the stomach (box drawn in the left panel). Nuclei were visualized with Hoechst. Antibodies against smooth muscle cells (γSMA), and neuronal cells (TUJ1) were used. Scale bars, 100 μm. (E) Light-sheet microscopy analysis after RapiClear tissue clearing and γSMA and TUJ1 immunofluorescence staining of E13 whole Control and *BAPX1*-expressing stomachs. Scale bars: 500 μm. White and red arrows indicate smooth muscle fiber organization in Control and *BAPX1*-expressing stomachs. (F) Virtual longitudinal sections of whole E13 *BAPX1*-expressing and Control stomachs stained for γSMA and TUJ1. White and red arrows indicate difference in circular muscle fiber orientation. Scale bars, 400 μm.

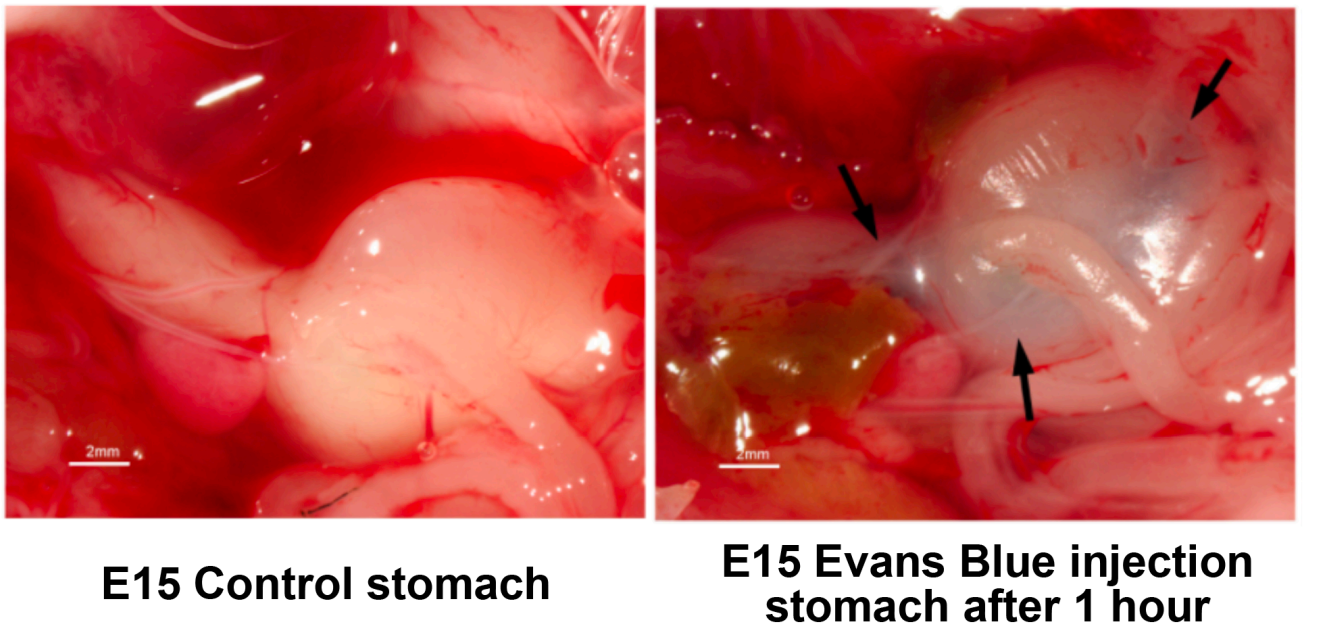

Fig. S1. Intra-oral administration of Evans Blue solution. After opening a small window in the extraembryonic membranes close to the head, the solution was deposited directly in the E15 chick embryo beak with a capillary pipette and the egg returned to the 38°C incubator. One hour later, the whole GI tract was dissected and the dye was observed in the stomach lumen (black arrows).

A

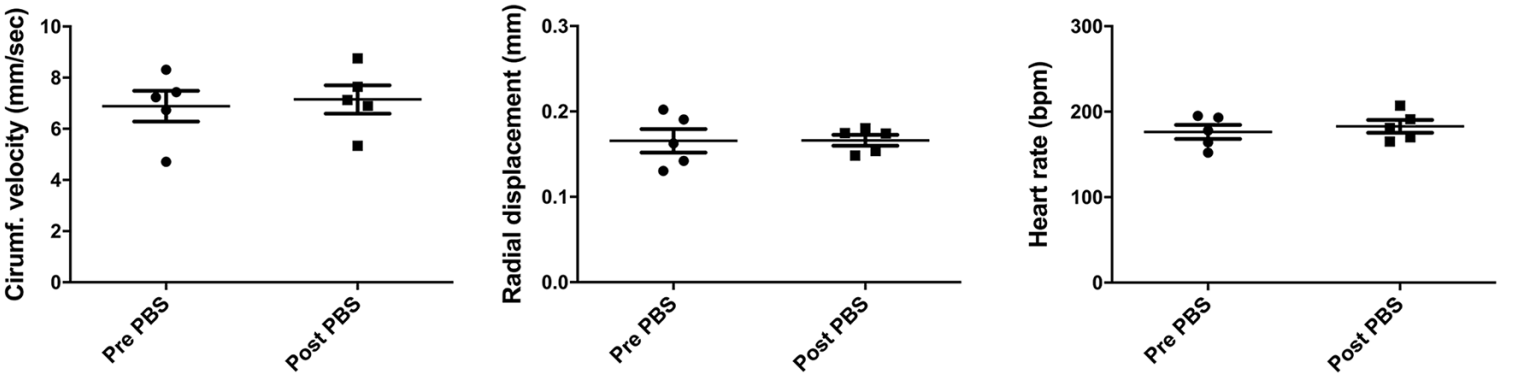
Circumf. velocity (mm/sec)
10
8
6
4
2
0
Pre PBS
Post PBS
Radial displacement (mm)
0.3
0.2
0.1
0.0
Pre PBS
Post PBS
Heart rate (bpm)
300
200
100
0
Pre PBS
Post PBS

B

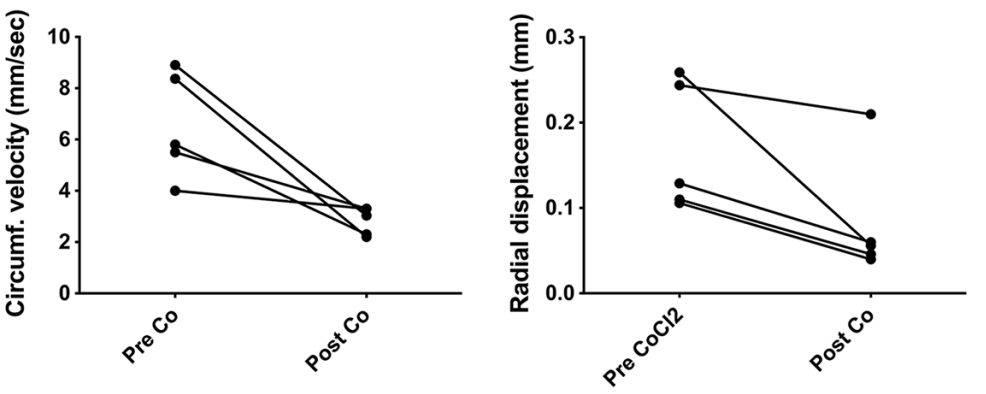
Circumf. velocity (mm/sec)
10
8
6
4
2
0
Pre Co
Post Co
Radial displacement (mm)
0.3
0.2
0.1
0.0
Pre CoCl2
Post Co

C

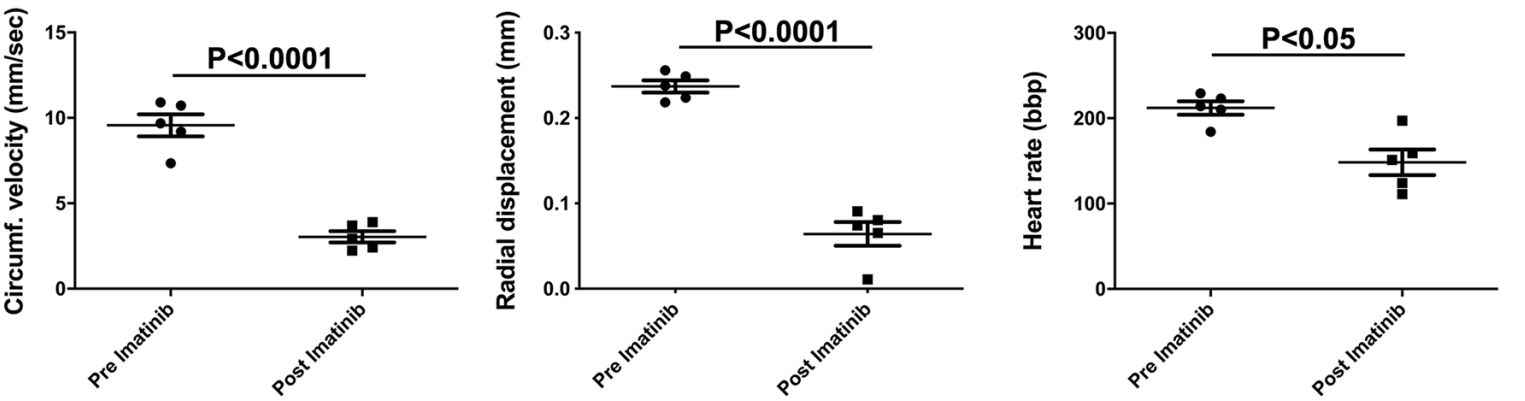
Circumf. velocity (mm/sec)
15
10
5
0
P<0.0001
Pre Imatinib
Post Imatinib
Radial displacement (mm)
0.3
0.2
0.1
0.0
P<0.0001
Pre Imatinib
Post Imatinib
Heart rate (bbp)
300
200
100
0
P<0.05
Pre Imatinib
Post Imatinib

D

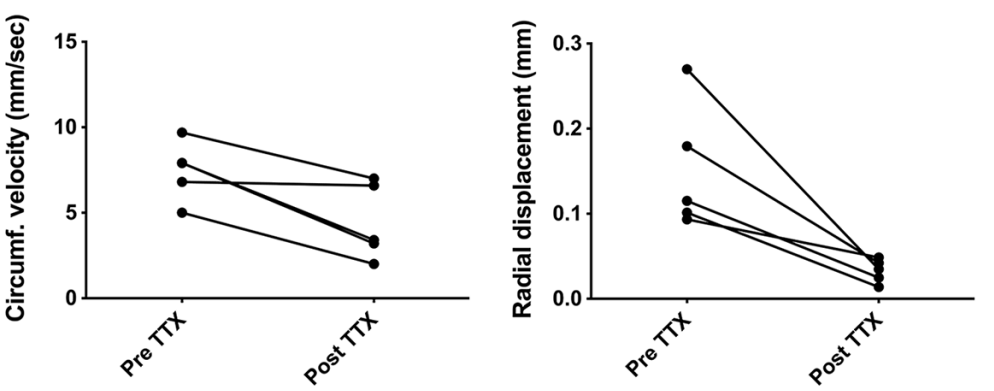
Circumf. velocity (mm/sec)
15
10
5
0
Pre TTX
Post TTX
Radial displacement (mm)
0.3
0.2
0.1
0.0
Pre TTX
Post TTX

Fig. S2. Impact of intra-oral administration of PBS and drugs on stomach motility. (A) Evaluation of the impact of intra-oral administration of PBS (negative control), compared to untreated, on the stomach circumferential strain velocity, stomach radial strain changes, and heart rate in E15 chick embryos (n=5). PBS administration did not alter the stomach circumferential velocity (from 6.88 ± 0.92 mm/sec before to 7.15 ± 0.83 mm/sec after PBS administration, not significant) and radial displacement (from 0.165 ± 0.02 mm before to 0.166 ± 0.012 mm after treatment, not significant) and the heart rate (176.4 ± 14.7 bpm before and 182.8 ± 12.9 bpm after treatment, not significant). (B) Changes of circumferential strain velocity and radial strain in individual stomachs before and after Cobalt Chloride (CoCl2) administration in E15 chick embryos (n=5). (C) Impact of imatinib (20 μM) on stomach circumferential strain velocity, stomach radial strain changes, and heart rate in E15 chick embryos (n=5). (D) Changes of circumferential strain velocity and radial strain in individual stomachs before and after tetrodotoxin (TTX) administration in E15 chick embryos (n=5).

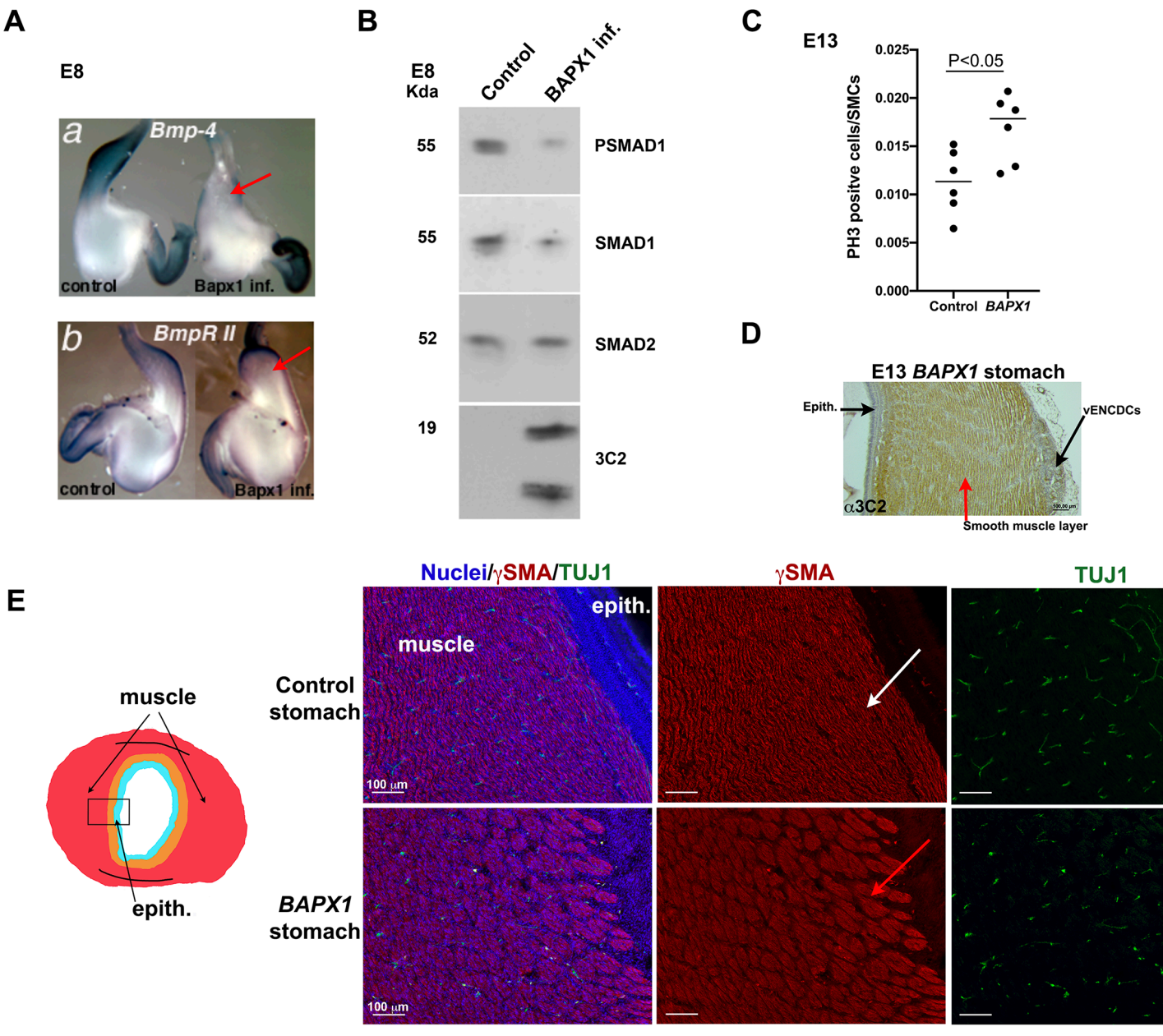

Fig. S3. Inhibition of BMP signaling activation in *BAPX1*-overexpressing stomach. (A) *In situ* hybridization analysis of whole-mount E8 stomach overexpressing BAPX1 demonstrated that BAPX1 leads to *BMP4* and *BMPRII* mRNA inhibition (red arrows in panels a, b). (B) Western blot analysis of protein extracts from E8 stomach overexpressing

BAPX1 showed inhibition of PSMAD1/5/8 (namely PSMAD1) and SMAD1 expression. (C) Quantification of PH3-positive cells in Control and the *BAPX1*-overexpressing stomach smooth muscle layer at E13. Proliferation rates were assessed by counting the number of PH3-positive cells relative to the total number of aSMA-positive nuclei in the section. Six control stomachs and six *BAPX1*-overexpressing stomachs were analyzed. One slide for each stomach was analyzed. *P<0.05 (Student's *t*-test). Mean ratio of PH3-positive cells/SMCs was 0.01130 (for Control) and 0.01681 (for BAPX1). Error bars indicate s.e.m. (D) Transversal paraffin sections of E13 *BAPX1*-expressing stomach analyzed by immunohistochemistry with an anti-gag (3C2) antibody. Red arrow indicates the presence of retroviral infection in the smooth muscle layer and black arrows its absence in the stomach epithelial layer and vENCDCs. Scale bars: 100μm. (E) Transversal paraffin sections of E13 *BAPX1*-expressing and Control stomachs close to the epithelium (box drawn in the left panel). Nuclei were visualized with Hoechst. Antibodies against smooth muscle cells (γSMA), and neuronal cells (TUJ1) were used. Scale bars, 100 μm.

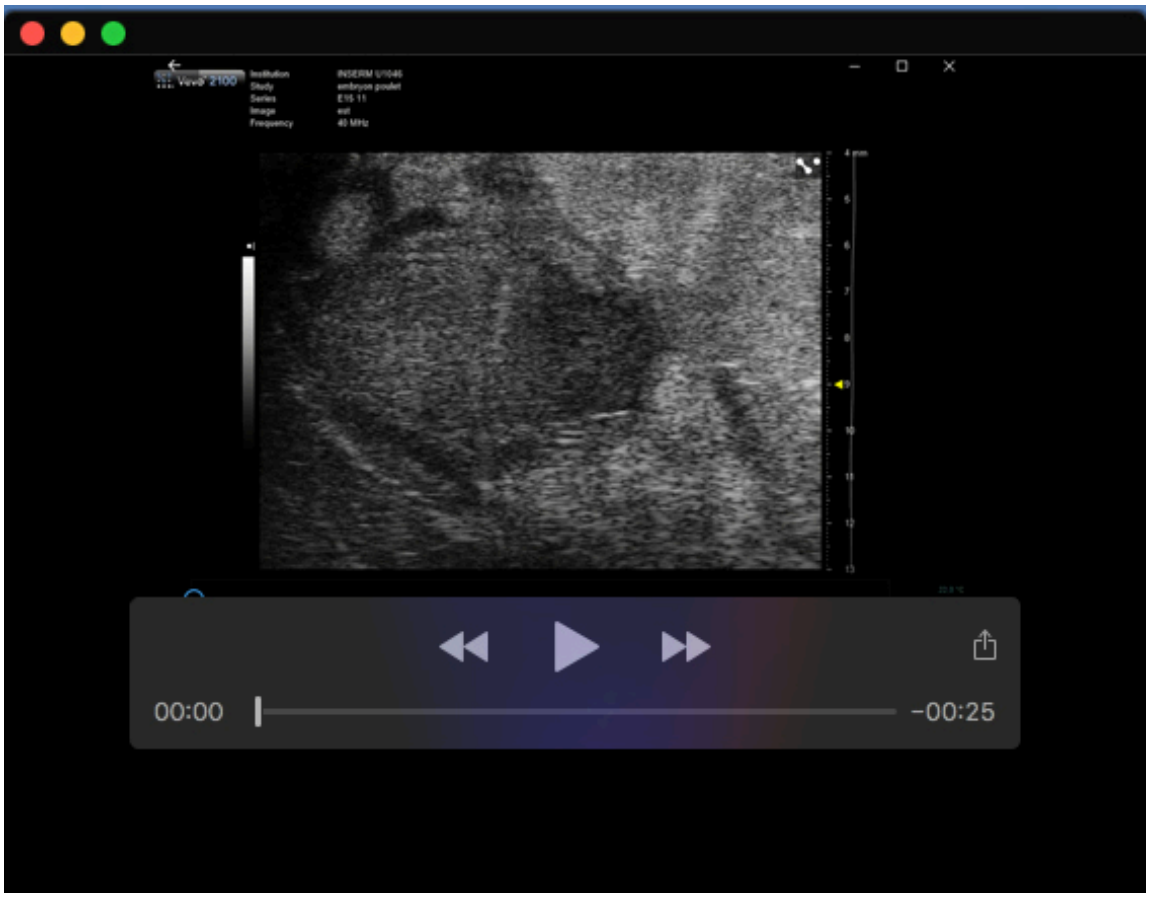

Movie 1. Movie obtained using the Vevo2100 ultrasound system to visualize stomach motility at E15.

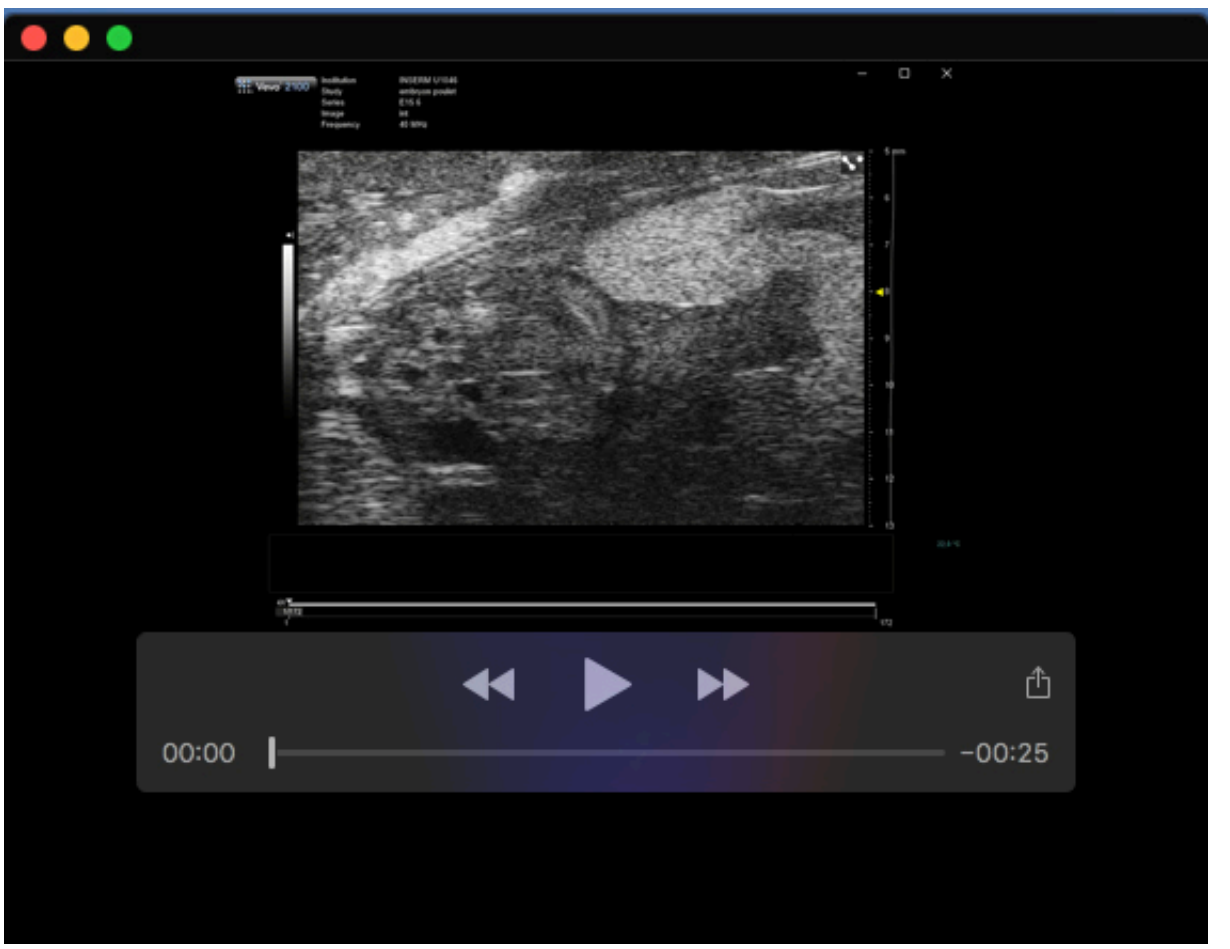

Movie 2. Movie obtained using the Vevo2100 ultrasound system to visualize small intestine motility at E15.

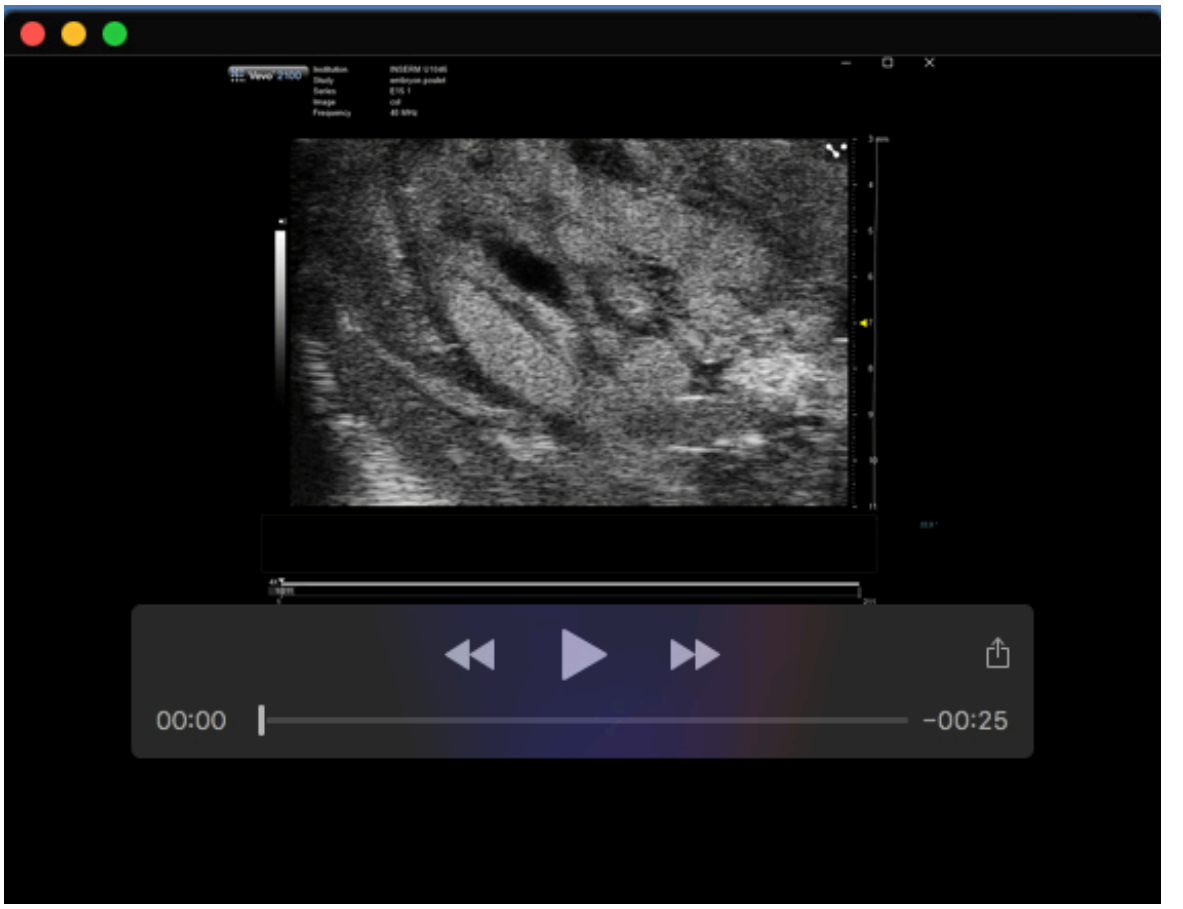

Movie 3. Movie obtained using the Vevo2100 ultrasound system to visualize colon motility at E15.

Movie 4. Movie obtained using the Vevo2100 ultrasound system to visualize stomach motility at E8.

Movie 5. Movie obtained using the Vevo2100 ultrasound system to visualize stomach motility at E13.

Movie 6. Movie obtained using the Vevo3100 ultrasound system to visualize stomach motility of E13 Control-stomach.

Movie 7. Movie obtained using the Vevo3100 ultrasound system to visualize stomach motility of E13 *BAPX1*-overexpressing stomach.

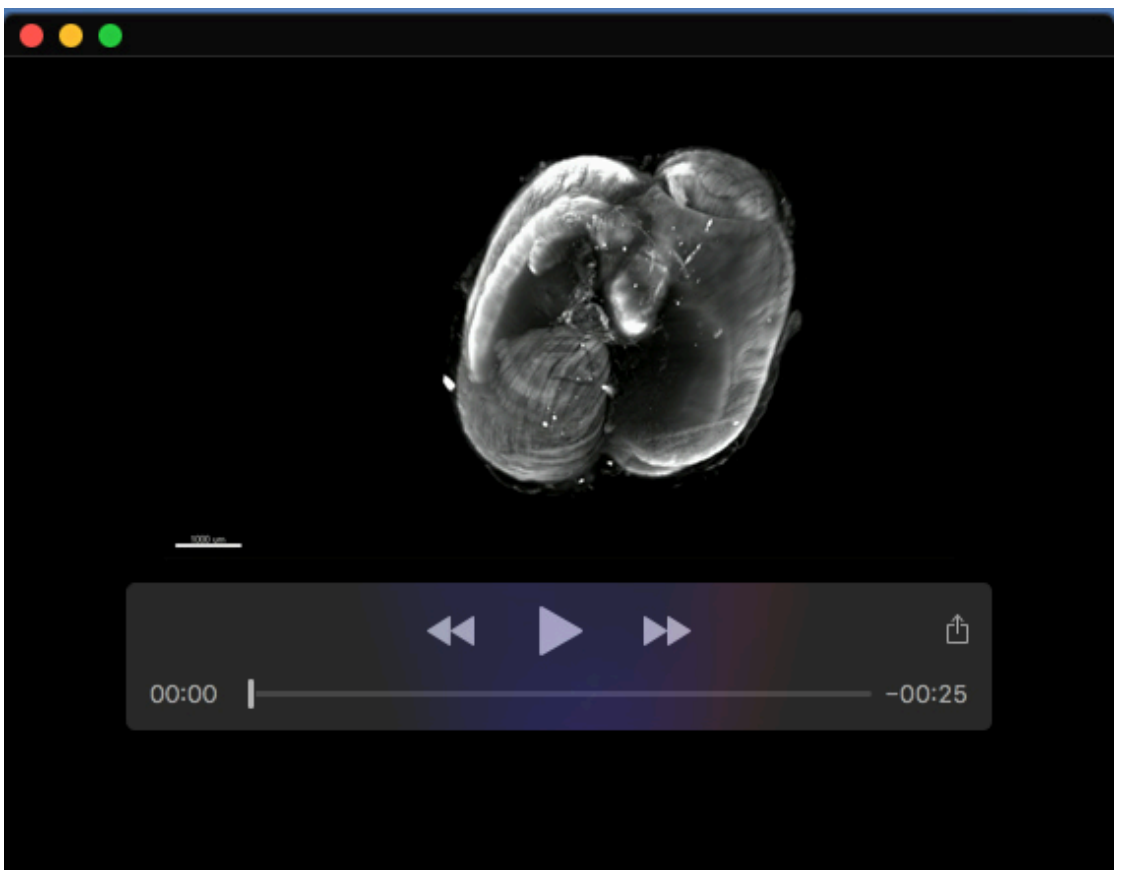

Movie 8. 3D Control stomach smooth muscle and ENS imaging at E13 using γSMA and TUJ1 immunofluorescence analysis.

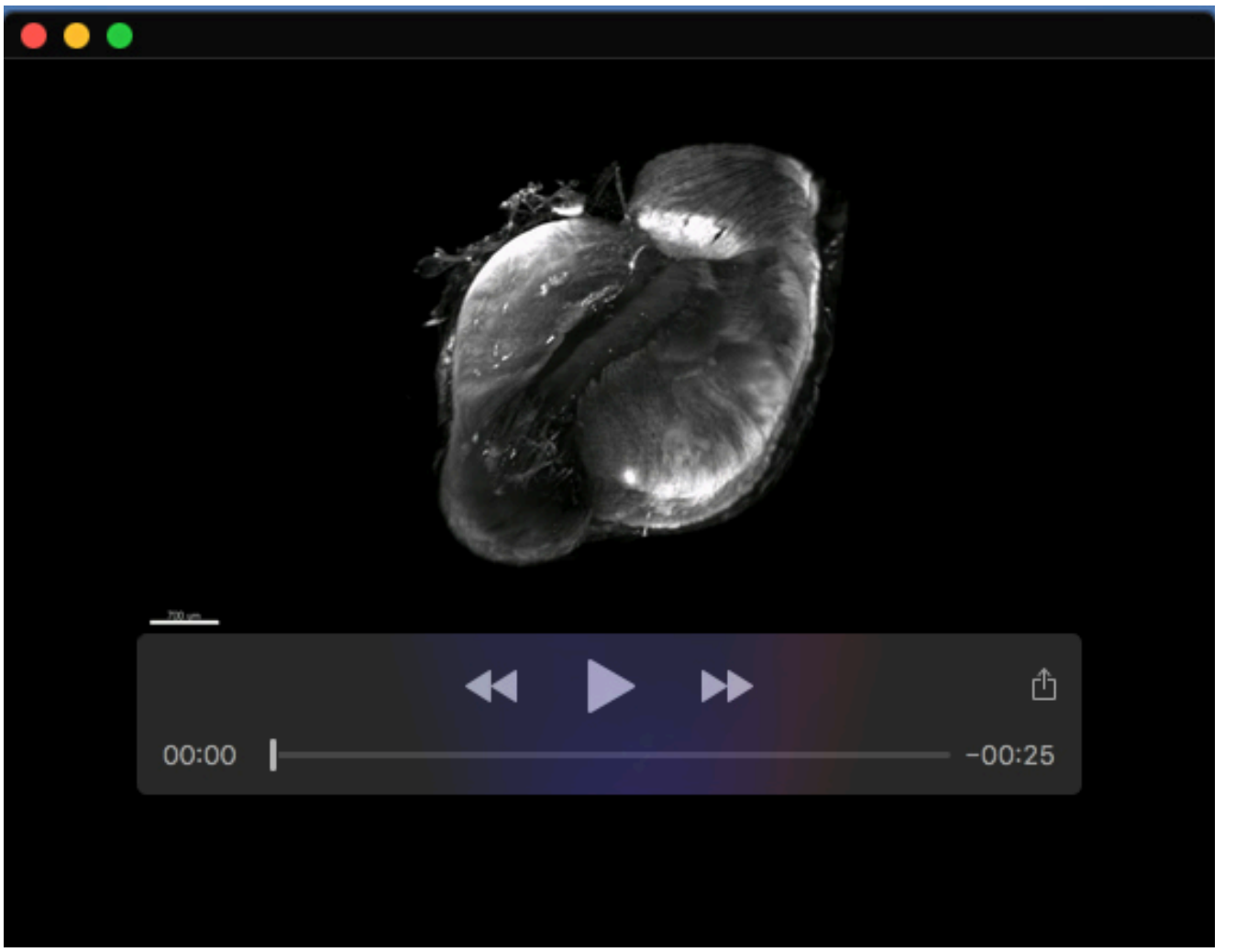

Movie 9. 3D *BAPX1*-overexpressing stomach smooth muscle and ENS imaging at E13 using γSMA and TUJ1 immunofluorescence analysis.